

Universität des Saarlandes



Fachrichtung 6.1 – Mathematik

Preprint Nr. 162

**Morphology for Matrix Data:
Ordering versus PDE-Based Approach**

Bernhard Burgeth, Andres Bruhn, Stephan Didas,
Joachim Weickert and Martin Welk

Saarbrücken 2005

Morphology for Matrix Data: Ordering versus PDE-Based Approach

Bernhard Burgeth

Mathematical Image Analysis Group
Faculty of Mathematics and Computer Science
Saarland University, Building E 24
66041 Saarbrücken, Germany
burgeth@mia.uni-saarland.de

Andres Bruhn

Mathematical Image Analysis Group
Faculty of Mathematics and Computer Science
Saarland University, Building E 24
66041 Saarbrücken, Germany
bruhn@dmia.uni-saarland.de

Stephan Didas

Mathematical Image Analysis Group
Faculty of Mathematics and Computer Science
Saarland University, Building E 24
66041 Saarbrücken, Germany
didas@mia.uni-saarland.de

Joachim Weickert

Mathematical Image Analysis Group
Faculty of Mathematics and Computer Science
Saarland University, Building E 24
66041 Saarbrücken, Germany
weickert@mia.uni-saarland.de

Martin Welk

Mathematical Image Analysis Group
Faculty of Mathematics and Computer Science
Saarland University, Building E 24
66041 Saarbrücken, Germany
welk@mia.uni-saarland.de

Edited by
FR 6.1 – Mathematik
Universität des Saarlandes
Postfach 15 11 50
66041 Saarbrücken
Germany

Fax: + 49 681 302 4443
e-Mail: preprint@math.uni-sb.de
WWW: <http://www.math.uni-sb.de/>

Abstract

Matrix fields are becoming increasingly important in digital imaging. In order to perform shape analysis, enhancement or segmentation of such matrix fields, appropriate image processing tools must be developed. This paper extends fundamental morphological operations to the setting of matrices, in the literature sometimes referred to as tensors despite the fact that matrices are only rank two tensors. The goal of this paper is to introduce and explore two approaches to mathematical morphology for matrix-valued data: One is based on a partial ordering, the other utilises nonlinear partial differential equations (PDEs).

We start by presenting definitions for the maximum and minimum of a set of symmetric matrices since these notions are the cornerstones of the morphological operations. Our first approach is based on the Loewner ordering for symmetric matrices, and is in contrast to the unsatisfactory component-wise techniques. The notions of maximum and minimum deduced from the Loewner ordering satisfy desirable properties such as rotation invariance, preservation of positive semidefiniteness, and continuous dependence on the input data.

These properties are also shared by the dilation and erosion processes governed by a novel nonlinear system of PDEs we are proposing for our second approach to morphology on matrix data. These PDEs are a suitable counterpart of the nonlinear equations known from scalar continuous-scale morphology. Both approaches incorporate information simultaneously from all matrix channels rather than treating them independently. In experiments on artificial and real medical positive semidefinite matrix-valued images we contrast the resulting notions of erosion, dilation, opening, closing, top hats, morphological derivatives, and shock filters stemming from these two alternatives. Using a ball shaped structuring element we illustrate the properties and performance of our ordering- or PDE-driven morphological operators for matrix-valued data.

Keywords: Mathematical morphology, dilation, erosion, matrix-valued images, diffusion tensor MRI, Loewner ordering, nonlinear partial differential equation

Introduction

0.1 Motivation and Short Overview

Mathematical morphology has met the needs of the image processing community for nearly four decades. The story of success has started in the

sixties with Serra's and Matheron's pioneering work on binary morphology [26, 35], and continued with generalisations to greyscale morphology in the eighties and proposed extensions of morphological concepts to vector-valued images and image sequences. The variety in mathematical morphology is well documented in many monographs, e.g. [20, 27, 36, 37, 38] and conference proceedings, e.g. [16, 21, 39, 25, 15].

Nevertheless, the treatment of *matrix-valued* images is still at its infancy, despite the fact that matrix fields have gained importance in recent years:

- First, *diffusion tensor magnetic resonance imaging (DT-MRI)* [4] is a modern but commonly used medical imaging technique that measures a 3×3 positive semidefinite matrix-field: A so-called diffusion tensor is assigned to each voxel. This diffusion tensor describes the diffusive property of water molecules. As such it reflects the geometry and organisation of the tissue under examination and is a very valuable tool for the diagnosis of multiple sclerosis and strokes [30].
- Second, the concept of tensors has been established as fruitful in image analysis itself [17]: The *structure tensor* [13], for instance, (also called Förstner interest operator, second moment matrix or scatter matrix) is used for corner detection [19], but also for motion [5] and texture analysis [31].
- Third, in civil engineering and solid mechanics anisotropic behaviour is often described satisfactorily by inertia, diffusion and permittivity tensors and stress-strain relationships

This variety of applications creates the need to develop appropriate tools for the processing and analysis of tensor respectively matrix data: As in the scalar case edges and shapes must be detected, noise removed and structures must be enhanced. Treating the channels independently is a strategy which is simple and close at hand. Along this line shift-invariant linear filters [44] and adaptive nonlinear filters [18] for DT-MRI data have been designed, with the drawback of ignoring any relation between the different matrix channels. More advanced approaches have been based on the smoothing of derived joint expressions such as the eigenvalues and eigenvectors of the matrix field [11, 40] or its fractional anisotropy [29]. Again this boils down to scalar- or/and vector-valued filtering with all its serious shortcomings.

Unlike vectors, matrices can be multiplied making, in effect, matrix-valued polynomials and even functions of matrices a very useful notion that decisively rely on the strong interplay between the different matrix entries. We

emphasise once more that in our opinion only concepts of morphological filters for matrix data that take full advantage of the rich algebraic structure offered by matrices will lead to convincing results.

Matrix-valued image processing methods that actually exploit the interaction of the different matrix channels have been introduced for nonlinear regularisation methods and related diffusion filters [40, 42]. The resulting nonlinear structure tensor [42] has shown its use in motion estimation [7], texture analysis [32] and unsupervised segmentation [6]. Matrix-channel interaction also is an essential part in the approaches to median filtering [43], to active contour and mean curvature motion models for tensor fields [12].

Encouraged by the numerous examples mentioned above where PDE-based filter techniques have been extended to the matrix-valued setting it seems worthwhile to search for a matrix-valued counterpart for PDE-driven greyscale morphology captured in (1).

0.2 Our Contribution

In [9] the basic operations dilation and erosion as well as opening and closing have been transferred to the matrix-valued setting at least for 2×2 matrices. However, the proposed approaches lack the continuous dependence on the input matrices which, confirmed by experiments, renders them useless for the design of morphological derivatives.

The novel approach in [10] using the so-called Loewner ordering for 2×2 matrices overcomes this inadequacy. The non-trivial extension to higher-order matrices has been achieved in [8] taking into account the detailed geometric structure of the cone associated with the Loewner ordering.

The goal of this article is two-fold: First, we present the approach to morphological operators for matrix-valued images based on the Loewner ordering. Second, we propose a novel matrix-valued analog of the nonlinear PDE (1). The results of the two approaches will be juxtaposed for a number of morphological operators ranging from the basic dilation/erosion over top-hats to morphological derivatives and Laplacian.

The morphological operations to be defined either via Loewner ordering or via nonlinear PDEs should work on the set $\text{Sym}(n)$ of symmetric $n \times n$ matrices and have to satisfy conditions such as:

- (i) Continuous dependence of the basic morphological operations on the matrices used as input for the aforementioned reasons,
- (iii) preservation of the positive semidefiniteness of the matrix field since DT-MRI data sets possess this property,

(iii) rotational invariance in each voxel:

$$V^\top \mathcal{MO}(A_1, \dots, A_n)V = \mathcal{MO}(V^\top A_1 V, \dots, V^\top A_n V) \quad \text{for any orthonormal matrix } V \text{ and where } \mathcal{MO} \text{ stands for a standard morphological operation.}$$

The article is structured as follows: The subsequent Section 1 gives a brief account of the morphological operations we aim to extend to the matrix-valued setting. In Section 2 we present the crucial maximum and minimum operations for matrix-valued data based on the Loewner ordering. Section 3 is devoted to the introduction and discussion of the matrix-valued counterpart of the nonlinear diffusion equation (1). The results of our experiments with various morphological operators employing the ordering or PDE approach will be juxtaposed in Section 4. We use artificial matrix-fields as test data for the sake of better comparability and judgment. The last Section 5 provides concluding remarks.

1 Morphological and Mathematical Preliminaries

In order to make this article as self-contained as possible we collect in this section basic definitions and facts from morphology, matrix theory, and convex analysis. The reader interested in a more detailed exposition is referred to the literature cited below.

1.1 Basic Flat Morphology

Standard morphological operations employ the so-called *structuring element* to work on images represented by scalar functions $f(x, y)$ with (x, y) in the image domain Ω , $(x, y) \in \Omega \subset \mathbb{R}^2$. Greyscale *dilation* \oplus , resp., *erosion* \ominus w.r.t. B is defined by

$$\begin{aligned} (f \oplus B)(x, y) &:= \sup \{f(x-x', y-y') \mid (x', y') \in B\}, \\ (f \ominus B)(x, y) &:= \inf \{f(x-x', y-y') \mid (x', y') \in B\}. \end{aligned}$$

The combination of dilation and erosion gives rise to various other morphological operators such as *opening* and *closing*,

$$f \circ B := (f \ominus B) \oplus B, \quad f \bullet B := (f \oplus B) \ominus B,$$

the *white top-hat* and its dual, the *black top-hat*

$$\text{WTH}(f) := f - (f \circ B), \quad \text{BTH}(f) := (f \bullet B) - f,$$

finally, the *self-dual top-hat*, $\text{SDTH}(f) := (f \bullet B) - (f \circ B)$.

The boundaries of objects are the loci of high greyvalue variations in an image which can be detected by gradient operators. The so-called *Beucher gradient*

$$\varrho_B(f) := (f \oplus B) - (f \ominus B),$$

as well as the *internal* and *external gradient*,

$$\varrho_B^-(f) := f - (f \ominus B), \quad \varrho_B^+(f) := (f \oplus B) - f$$

are analogs to the norm of the gradient $\|\nabla f\|$ if f is considered as a differentiable image.

The application of shock filtering to matrix-valued data calls for an equivalent of the Laplace operator $\Delta f = \partial_{xx}f + \partial_{yy}f$ appropriate for this type of data. A *morphological Laplacian* has been introduced in [41]. However, we use a variant given by

$$\Delta_B f := \varrho_B^+(f) - \varrho_B^-(f) = (f \oplus B) - 2 \cdot f + (f \ominus B).$$

This form of a Laplacian acts as the second derivative $\partial_{\eta\eta}f$ where η stands for the direction of the steepest slope. Therefore it allows us to distinguish between influence zones of minima and maxima of the image f , a property essential for the design of shock filters.

The idea underlying *shock filtering* is applying either a dilation or an erosion to an image, depending on whether the pixel is located within the influence zone of a minimum or a maximum [24]:

$$S_B f := \begin{cases} f \oplus B, & \text{trace}(\Delta_B f) < 0, \\ f, & \text{trace}(\Delta_B f) = 0, \\ f \ominus B, & \text{trace}(\Delta_B f) > 0. \end{cases}$$

1.2 Continuous Morphology

In ([34, 33]) nonlinear partial differential equations were proposed that mimic the process of dilation and erosion. For flat morphology with a ball as structuring element this diffusion equation reads

$$\partial u_t = \pm \|\nabla u\|, \tag{1}$$

with initial condition $u(x, y, 0) = f(x, y)$. Here f is the original image on the image domain Ω and u its transformed versions. The PDE framework for morphology has its advantages: The sophisticated machinery of numerical solution methods for PDEs is at our disposal and, most important, this continuous approach allows for sub-pixel accuracy.

1.3 Convex Matrix Analysis

The set $\text{Sym}(n)$ of symmetric $n \times n$ -matrices with real entries is a vector space w.r.t. the usual rules for summation and multiplication by a scalar. $\text{Sym}(n)$ is endowed with the scalar product $\langle A, B \rangle := \sqrt{\text{trace}(A^\top B)}$ giving rise to the Frobenius norm for matrices: $\|A\| = \sqrt{\sum_{i,j=1}^n a_{ij}^2}$.

Symmetric matrices can be regarded as a generalisation of real numbers and one can define functions h of those matrices [23]: Let $\text{diag}(\alpha_1, \dots, \alpha_n)$ denote a diagonal matrix with entries $\alpha_1, \dots, \alpha_n$. We define for a symmetric matrix $A \in \text{Sym}(n)$ with eigenvalue decomposition $A = V \text{diag}(\alpha_1, \dots, \alpha_n) V^\top$ and orthogonal matrix V the matrix $h(A)$ by

$$h(A) := V \text{diag}(h(\alpha_1), \dots, h(\alpha_n)) V^\top \quad (2)$$

provided the α_i 's lie in the domain of definition of h . We observe that this definition is rotational invariant and preserves symmetry, $h(A) \in \text{Sym}(n)$.

The following example is of great importance for the subsequent exposition: Specifying h as the absolute value function, $h(x) = |x|$ associates with a matrix A its absolute value $|A|$. This $|A|$ denotes a positive semidefinite matrix and must not be confused with the norm or determinant of A .

Symmetric matrices A that satisfy $x^\top A x \geq 0$ for all $x \in \mathbb{R}^n$ are commonly called *positive semidefinite*. This gives rise to a natural partial ordering on $\text{Sym}(n)$, the so-called *Loewner ordering* defined via the set of positive semidefinite matrices $\text{Sym}^+(n)$ by

$$A, B \in \text{Sym}(n) : \quad A \geq B :\Leftrightarrow A - B \in \text{Sym}^+(n),$$

i. e. $A \geq B$ if and only if $A - B$ is positive semidefinite.

The notions of maximal and minimal matrices to be introduced in the following chapter will rely on the Loewner ordering. This makes it necessary to give a brief account of some notions from convex analysis, for more details the reader is referred to [2, 22], for example.

A subset C of a vector space V is called *cone*, if it is stable under addition and multiplication with a positive scalar. Hence, the set $\text{Sym}^+(n)$ of positive definite matrices is a cone, the ordering cone associated with the Loewner ordering.

A subset B of a cone C is named *base* if every $y \in C, y \neq 0$ admits a unique representation as $y = r \cdot x$ with $x \in B$ and $r > 0$. For instance, the set of positive semidefinite matrices with trace 1 form a base of $\text{Sym}^+(n)$. Observe that this base $\{M \in \text{Sym}^+(n) : \text{trace}(M) = 1\}$ is convex and compact.

By far the most important points of a compact convex set are its *extreme points* which can be characterised as follows: A point x is an extreme point

of a convex subset $S \subset V$ of a vector space V if and only if $S \setminus \{x\}$ remains convex.

The set of all extreme points of S is denoted $\text{ext}(S)$. All extreme points are necessarily boundary points, $\text{ext}(S) \subset \text{bd}(S)$. The importance of the extreme points becomes apparent in the theorems of Minkowski and Krein-Milman which state that each convex compact set S in a finite dimensional vector space can be reconstructed as the set of all finite convex combinations of its extreme points [2, 22]:

$$\begin{aligned} S &= \text{convexhull}(\text{ext}(S)) \\ &= \left\{ \sum_{i=1}^N \lambda_i e_i \mid N \in \mathbb{N}, e_i \in \text{ext}(S), \lambda_i \geq 0, \text{ for } i = 1, \dots, N, \sum_{i=1}^N \lambda_i = 1 \right\} \end{aligned}$$

All the important information of a convex compact set is captured in its extreme points.

The (topological) interior of $\text{Sym}^+(n)$ is the cone of positive definite matrices, while its boundary consists of all matrices in $\text{Sym}^+(n)$ with a rank strictly smaller than n . It is known [2] that the matrices $v v^\top$ with unit vectors $v \in \mathbb{R}^n$, $\|v\| = 1$ are the extreme points of the base of $\text{Sym}^+(n)$. They have by construction rank 1 and for any unit vector v we find $v v^\top v = v \cdot \|v\|^2 = v$ which implies that 1 is the only non-zero eigenvalue, entailing $\text{trace}(v v^\top) = 1$. Because of this extremal property the matrices $v v^\top$ with $\|v\| = 1$ carry the complete information about the base of Loewner ordering cone and hence the cone itself: $\text{convexhull}(\{v v^\top : v \in \mathbb{R}^n, \|v\| = 1\})$ is a base for the Loewner ordering cone.

The concepts mentioned above can be visualised in the case $n = 2$, since it is possible to embed $\text{Sym}(2)$ in \mathbb{R}^3 via the mapping

$$A = (a_{ij})_{i,j=1,2} \longleftrightarrow \frac{1}{\sqrt{2}} (2a_{12}, a_{22} - a_{11}, a_{22} + a_{11})^\top.$$

The transform is an isometry and maps $\{A \in \text{Sym}(2) : \text{trace}(A) = 0\}$ onto the x-y-plane. In figure 1 (a) the the image of the cone for the Loewner ordering is indicated.

Manipulations with this ordering cone will put us in the position to define suitable notions for maximal and minimal matrices of a given finite set of symmetric matrices.

2 Morphology for Tensor Fields via Ordering

Before proceeding to define suitable notions for maximum and minimum of a set of matrices it is essential to clarify what ‘‘suitable’’ means. To do so we

will focus on a modern medical image acquisition technique: Diffusion tensor magnetic resonance imaging, DT-MRI.

This method measures the probability density function of displacements of particles that are subject to a Brownian motion within a sample material. The structure of material determines the movability of the particles, which is reflected in properties of this probability density. In biomedical DT-MRI the particles under consideration are water molecules performing random movements in biological tissue due to thermal fluctuations. In a first approximation the probability distributions are assumed to be Gaussian determined by positive semidefinite co-variance matrices Σ and zero mean. The corresponding *isoprobability surfaces* describe the diffusion. They depend on the quadratic form associated with Σ , $\{x \in \mathbb{R}^3 : x^\top \Sigma^{-2} x = 1\}$, and hence they are ellipsoids. In this respect the ellipsoids correspond exactly to the well-known orbits of electrons in atoms or molecules.

The shape of the ellipsoid provides information about hindering and enhancing influences on the diffusion of water molecules at a voxel and therefore about the underlying microstructure of the tissue. The maximal ellipsoid/matrix of a finite set of ellipsoids/matrices $\{E_i : i = 1, \dots, n\}$ should now reflect, in a minimal manner, the diffusion of a water molecule that underlies all the enhancing influences represented by the E_i . Likewise for the minimal ellipsoid/matrix: It should mirror all the hindering influences represented by E_i .

In other words, the maximal ellipsoid should be as small as possible and *cover* all E_i while the minimal ellipsoid should be as large as possible and be *contained* in all E_i .

The maximal and minimal matrices in general will not belong to the set of matrices they are bounding, and in view of the interpretation as isoprobability surfaces, this would not even be desirable for DT-MRI data.

It is important to remark, that this rules out the straightforward component-wise approach: It would lead to notions of maximal/minimal matrices whose corresponding ellipsoids fulfill neither the “covering“ nor the “containing“ property just mentioned.

For detailed information about the acquisition of DT-MRI data the reader might consult [3] or more recently, [1] and the literature cited therein.

Note that since the Loewner ordering for symmetric matrices solely relies on quadratic forms, it is a natural concept to consider, and we will do so in the next subsection.

2.1 Maximal and Minimal Matrices in the Loewner Ordering

The ordering cone of the Loewner ordering by definition consists of all the matrices that are larger than the zero-matrix at its vertex. A reverted and translated version of this cone then characterises the matrices that are smaller than the matrix marking its vertex; the *penumbra* $P(M)$ of a matrix $M \in \text{Sym}(n)$ is the set of matrices N that are smaller than M w.r.t. the Loewner ordering:

$$P(M) := \{N \in \text{Sym}(n) : N \leq M\} = M - \text{Sym}^+(n),$$

where we used the customary notation $a + rS := \{a + r \cdot s : s \in S\}$ for a point $a \in V$, a scalar $r \in \mathbb{R}$ and a subset $S \subset V$.

Using this geometric description the problem of finding the maximum of a set of matrices $\{A_1, \dots, A_m\}$ amounts to determining the minimal penumbra covering their penumbras $P(A_1), \dots, P(A_m)$. Its vertex represents the maximal matrix \bar{A} we are searching for and that dominates all A_i w.r.t the Loewner ordering.

However, the cone itself is too complicated a structure to be handled directly. Instead we associate with each matrix $M \in \text{Sym}(n)$ a *ball* in the subspace $\{A : \text{trace}(A) = 0\}$ of all matrices with zero trace as a *completely descriptive set*. For the sake of simplicity we will assume that $\text{trace}(M) \geq 0$. The enclosing ball is constructed in two steps: First, from the statements above we conclude that the set $\{M - \text{trace}(M) \cdot \text{convexhull}\{v v^\top : v \in \mathbb{R}, \|v\| = 1\}\}$ is a base for $P(M)$ contained in the subspace $\{A : \text{trace}(A) = 0\}$. We observe that the identity matrix E is perpendicular to the matrices A from this subspace, $\langle A, E \rangle = \sqrt{\text{trace}(A)} = 0$, and hence the orthogonal projection of M onto $\{A : \text{trace}(A) = 0\}$ is given by

$$m := M - \frac{\text{trace}(M)}{n} E. \quad (3)$$

Second, the extreme points of the base of $P(M)$ are lying on a sphere with center m and radius

$$r := \|M - \text{trace}(M)v v^\top - m\| = \text{trace}(M) \sqrt{1 - \frac{1}{n}}. \quad (4)$$

Consequently, if the center m and radius r of a sphere in $\{A \in \text{Sym}(n) : \text{trace}(A) = 0\}$ are given the vertex M of the associated penumbra $P(M)$ is obtained by

$$M = m + \frac{r}{n} \frac{1}{\sqrt{1 - \frac{1}{n}}} E. \quad (5)$$

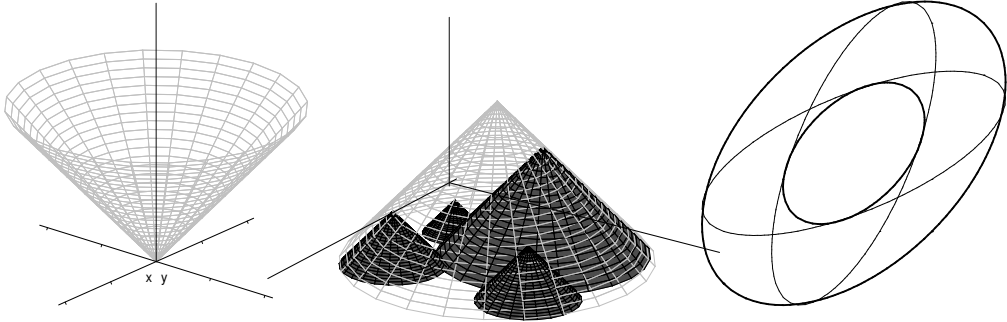


Figure 1: **(a) Left:** Image of the Loewner cone $\text{Sym}^+(2)$. **(b) Middle:** Cone covering four penumbras of other matrices. The tip of each cone represents a symmetric 2×2 matrix in \mathbb{R}^3 . Each of the cones (and hence its generating matrix) is uniquely determined by its circular base. The minimal disc covering the smaller discs belongs to the selected maximal matrix \bar{A} . **(c) Right:** The maximum (largest ellipse) and minimum (smallest ellipse) of two 2×2 -matrices.

With this information at our disposal, we can reformulate the task of finding a suitable maximal matrix \bar{A} dominating the matrices $\{A_1, \dots, A_m\}$: The *smallest* sphere enclosing the spheres associated with $\{A_1, \dots, A_m\}$ determines the matrix \bar{A} that dominates the A_i . It is minimal in the sense, that there is no smaller one w.r.t. the Loewner ordering which has this “covering property” of its penumbra.

This is a non-trivial problem of computational geometry and we tackle it by using a sophisticated algorithm implemented by B. Gaertner [14]. Given a set of points in \mathbb{R}^d it is capable of finding the smallest ball enclosing these points. Hence for each $i = 1, \dots, m$ we sample within the set of extreme points $\{A_i - \text{trace}(A_i)vv^\top\}$ of the base of $P(A_i)$ by expressing v in 3d-spherical coordinates, $v = (\sin \phi \cos \psi, \sin \phi \sin \psi, \cos \phi)$ with $\phi \in [0, 2\pi[$, $\psi \in [0, \pi[$.

Again we have the opportunity of visualisation in the case of 2×2 -matrices. Then the extreme points are the matrices vv^\top with $v^\top = (\cos \varphi, \sin \varphi)$ where $\varphi \in [0, 2\pi[$. Hence the aforementioned descriptive sets are discs in the x-y-plane determining the penumbras associated with the set of matrices. The penumbras of the matrices $\{A_1, \dots, A_m\}$ are covered with the minimal penumbral cone whose vertex represents the desired maximal matrix \bar{A} , see figure 1 (b). This minimal cone is found by calculating the smallest circle, its descriptive set, enclosing the discs stemming from the matrices $\{A_1, \dots, A_m\}$. The geometric point of view allows us to connect the maximum of matrices

w.r.t. the Loewner ordering to the maximum of real numbers. To this end recall the formula

$$\max(a_1, a_2) = \frac{1}{2}(a_1 + a_2) + \frac{1}{2}|a_1 - a_2| \quad (6)$$

valid for any real numbers a_1 and a_2 . Then an elementary calculation, furnishing the smallest enclosing sphere of two spheres, reveals that the maximal matrix dominating A_1 and A_2 obtained through

$$\max(A_1, A_2) = \frac{1}{2}(A_1 + A_2) + \frac{1}{2}|A_1 - A_2| \quad (7)$$

indeed coincides with the maximal matrix induced by the Loewner ordering. Note that an extension of this algebraic approach to sets of symmetric matrices with more than two elements is not feasible. Formula 7 and the corresponding expression for the minimum will play a vital role in the PDE-framework for morphology.

Let us summarise the above construction in four steps: In order to determine the maximal matrix \overline{A} to a given set of matrices $\{A_1, \dots, A_m\}$

1. calculate their projections a_i , $i = 1, \dots, m$ according to (3),
2. determine the radii r_i , $i = 1, \dots, m$, of the bases of their penumbras through (4),
3. determine the centre and radius of the smallest ball enclosing these bases,
4. recover the vertex of the associated penumbral cone via formula (5).

The minimal element \underline{A} is obtained through the formula

$$\underline{A} = (\max(A_1^{-1}, \dots, A_m^{-1}))^{-1}$$

inspired by its well-known counterpart for real numbers. The construction of maximal and minimal elements ensures their rotational invariance, their positive semidefiniteness and continuity. These properties are passed on to the above mentioned morphological operations.

3 PDE-Based Morphology for Tensor Fields

3.1 Matrix-Valued PDEs for Dilation and Erosion

As mentioned in the introduction the nonlinear PDEs that create a dilation and erosion process corresponding to a ball-shaped structuring element for

greyvalue images are given in [34] and read

$$\partial u_t = \pm \|\nabla u\| = \pm \sqrt{|\partial_x u|^2 + |\partial_y u|^2 + |\partial_z u|^2} \quad (8)$$

with initial condition $u(x, y, z, t) = f(x, y, z)$. This equation contains the gradient operator $\nabla := (\partial_x, \partial_y, \partial_z)^\top$ with its partial derivatives and the Euclidean vector norm $\|(v_1, v_2, v_3)^\top\| := \sqrt{v_1^2 + v_2^2 + v_3^2}$. For both we have to find suitable analogs for matrices.

It is important **not** to consider a matrix norm as the extension of the vector norm in (8). We rather give the expressions on the right hand side of (8) a new meaning in the framework of symmetric matrices aiming at a truly matrix-valued nonlinear partial differential equation as the counterpart of the scalar PDE (8).

To this end we have to clarify what a partial derivative, the absolute value and a square root of a symmetric matrix is.

We define the equivalent $\bar{\partial}_\alpha$ of the partial derivative ∂_α , spatial or temporal, of a scalar function for a matrix-valued function $U(x, y, z, t) = (U_{i,j})_{i,j=1,\dots,n}$ by componentwise application of ∂_α :

$$\bar{\partial}_\alpha U := (\partial_\alpha U_{i,j})_{i,j=1,\dots,n} \quad (9)$$

Due to the linearity of matrix multiplication and differentiation the application of $\bar{\partial}_\alpha$

- preserves symmetry: $U \in \text{Sym}(n) \implies \bar{\partial}_\alpha U \in \text{Sym}(n)$,
- is rotational invariant:
 $\bar{\partial}_\alpha(WUW^\top) = W(\bar{\partial}_\alpha U)W^\top$ holds for any constant orthogonal matrix W .

We remember the definition of a function of a symmetric matrix given in 2. Then, by using the specifications $h(x) = |x|^2$ and $h(x) = \sqrt{x}$, we have equipped the matrix-valued expression $\sqrt{|\bar{\partial}_x U|^2 + |\bar{\partial}_y U|^2 + |\bar{\partial}_z U|^2}$ with meaning. With this at our disposal it is now possible to establish the matrix-valued counterpart of (8):

$$\bar{\partial} U_t = \pm \sqrt{|\bar{\partial}_x U|^2 + |\bar{\partial}_y U|^2 + |\bar{\partial}_z U|^2} \quad (10)$$

where “+” governs the dilation-like, and “-” rules the erosion-like diffusion process.

The expression on the right again is rotational invariant and produces positive, resp., negative semidefinite matrices depending on the choice of the positive, resp., negative sign. Equation (10) truly exploits the matrix structure of the data since it describes a highly correlated system of nonlinear partial differential equations in $n \times n$ unknowns.

3.2 A Matrix-Valued Variant of the Osher-Sethian-Scheme

Inspired by numerical schemes for hyperbolic conservation laws Osher and Sethian [28] proposed for the two-dimensional scalar dilation equation $\partial_t u = \sqrt{(\partial_x u)^2 + (\partial_y u)^2}$ the numerical approximation

$$\begin{aligned} \frac{u(i, j)^{(n+1)} - u(i, j)^{(n)}}{\tau} &= \\ &= \left[\left(\min \left(\frac{u(i, j)^{(n)} - u(i-1, j)^{(n)}}{h_1}, 0 \right) \right)^2 + \left(\max \left(\frac{u(i+1, j)^{(n)} - u(i, j)^{(n)}}{h_1}, 0 \right) \right)^2 \right. \\ &+ \left. \left(\min \left(\frac{u(i, j)^{(n)} - u(i, j-1)^{(n)}}{h_2}, 0 \right) \right)^2 + \left(\max \left(\frac{u(i, j+1)^{(n)} - u(i, j)^{(n)}}{h_2}, 0 \right) \right)^2 \right]^{1/2} \\ &= \left[\left(\left(\frac{u(i, j)^{(n)} - u(i-1, j)^{(n)}}{h_1} \right)^- \right)^2 + \left(\left(\frac{u(i+1, j)^{(n)} - u(i, j)^{(n)}}{h_1} \right)^+ \right)^2 \right. \\ &+ \left. \left(\left(\frac{u(i, j)^{(n)} - u(i, j-1)^{(n)}}{h_2} \right)^- \right)^2 + \left(\left(\frac{u(i, j+1)^{(n)} - u(i, j)^{(n)}}{h_2} \right)^+ \right)^2 \right]^{1/2}. \end{aligned}$$

where, for instance, $u(i, j)^{(n)}$ stands for the value of the function u at $(i \cdot h_1, j \cdot h_2)$ at n -th time step of size τ . We have also used the abbreviations $u^+ = \max(u, 0)$ and $u^- = \min(u, 0)$. Aside from the obvious extension to three dimensions we realise, that this scheme can be reinterpreted in terms of symmetric matrices:

The scheme requires to perform subtractions and scalar multiplications, to rise to the power of 2, to take the square roots, and to determine the maximum and minimum of two matrices. With the preparations in the subsection above all these operations are at our disposal also in the case of symmetric matrices. So we are allowed to replace the scalar function u by the $n \times n$ matrix U to obtain a matrix-valued scheme for the matrix-valued PDE (10):

$$\begin{aligned}
& \frac{U(i, j, k)^{(n+1)} - U(i, j, k)^{(n)}}{\tau} = \\
& = \left[\left(\left(\frac{U(i, j, k)^{(n)} - U(i-1, j, k)^{(n)}}{h_1} \right)^- \right)^2 + \left(\left(\frac{U(i+1, j, k)^{(n)} - U(i, j, k)^{(n)}}{h_1} \right)^+ \right)^2 \right. \\
& + \left(\left(\frac{U(i, j, k)^{(n)} - U(i, j-1, k)^{(n)}}{h_2} \right)^- \right)^2 + \left(\left(\frac{U(i, j+1, k)^{(n)} - U(i, j, k)^{(n)}}{h_2} \right)^+ \right)^2 \\
& \left. + \left(\left(\frac{U(i, j, k)^{(n)} - U(i, j, k-1)^{(n)}}{h_3} \right)^- \right)^2 + \left(\left(\frac{U(i, j, k+1)^{(n)} - U(i, j, k)^{(n)}}{h_3} \right)^+ \right)^2 \right]^{1/2}.
\end{aligned}$$

It is convenient to use formula (7) to calculate the maximum and its well-known analog $\min(A_1, A_2) = \frac{1}{2}(A_1 + A_2 - |A_1 - A_2|)$ to calculate the minimum of two matrices $A_1, A_2 \in \text{Sym}(n)$.

The numerical approximation for the PDE of the erosion differs from the one for dilation only by a factor -1 and the exchange of minimum and maximum operations. Hence it poses no further challenge and a detailed exposition is skipped here for the sake of brevity.

4 Experimental Results and their Comparison

In our numerical experiments we use an artificial $20 \times 20 \times 20$ -field as well as an $128 \times 128 \times 30$ field of 3-D positive definite matrices originating from a 3-D DT-MRI data set of a human head, see figures 2, 7.

The data are represented as ellipsoids via the level sets of the quadratic form $\{x^\top A x : x \in \mathbb{R}^3\}$ associated with a matrix $A \in \text{Sym}^+(3)$. In using A^{-2} the length of the semi-axes of the ellipsoid correspond directly with the three eigenvalues of the positive definite matrix.

The artificial data constitute a cross-like structure where the ellipsoids in the center of the cross are lense-shaped, the ones in the arms of the cross are strongly elongated, while those outside the cross are simple balls.

For the ordering-based morphological operators a ball-shaped structuring element of radius 2, in the sequel abbreviated by BSE(2), was used. As pointed out in the previous section 3.2 the proposed matrix partial differential equations (10) are solved numerically by a matrix-valued version of the Osher-Sethian-scheme for dilation and erosion.

In general 4 iterations with a time step size of 0.5 were performed, resulting in a stopping time of 2 which corresponds to the size of the structuring element.

In the scalar setting the diffusion processes governed by (8) are followed by a threshold operation. However, we refrained from doing so in order to avoid additional parameters and their arbitrariness, especially in the matrix-valued setting. The price to pay will be the presence of blurring, since the Osher-Sethian-scheme already creates blurring in the scalar case, and one cannot expect any better in the more complicated matrix-valued setting.

Due to the complexity of the not yet fully optimised procedures the running time to obtain dilation and erosion is about two orders of magnitude longer than in the case of comparable calculations with grey value data.

This blurring effect of the the numerical scheme is responsible for discrepancies in the experimental results for the artificial data in the case of closing and opening operations, figure 3, and consequently also in the case of the top hat operations, figure 4. However, this discrepancy is not as prominent for the medical images as can be seen in figures 8 and 9.

The image at the top of figure 2 displays the central slice of the original data cube where the z-direction is perpendicular to the image plane. Figure 7 (a) exhibits a 128×128 layer of the medical data while (b) displays an enlarged section near the upper right corner of (a).

In both cases the images below show the effect of dilation and erosion with both the ball-shaped structuring element BSE(2) and their imitations with the nonlinear PDEs (10). The results of both approaches are quite similar and reasonable. As it is expected from scalar-valued morphology, the shape of details in the dilated and eroded images correspond to the shape and size of the structuring element.

Clearly visible in the images of the right column of figures 2 and 7 is the blurring effect of the PDE-based approach. In view of the diffusive properties of the Osher-Sethian scheme, this does not come as a surprise.

However, we believe this blurring effect of the the numerical scheme to be responsible for discrepancies in the experimental results concerning the artificial data in the case of closing and opening operations, figure 3, and consequently also in the case of the top hat operations, figure 4. However, this discrepancy is not as prominent for the medical images as can be seen in figures 8 and 9. Obviously the concatenation of dilation and erosion enhances the negative effects of the blurring introduced by the numerical scheme.

Fortunately, when it comes to the Beucher gradient as well as the internal and the external gradient, the results from both approaches offer a striking similarity. As visible in figures 5 and 10 the gradients (especially the one-sided gradients) stemming from both approaches are able to detect edge-like features. The PDE-based results look like slightly blurred versions of the ordering based outcome.

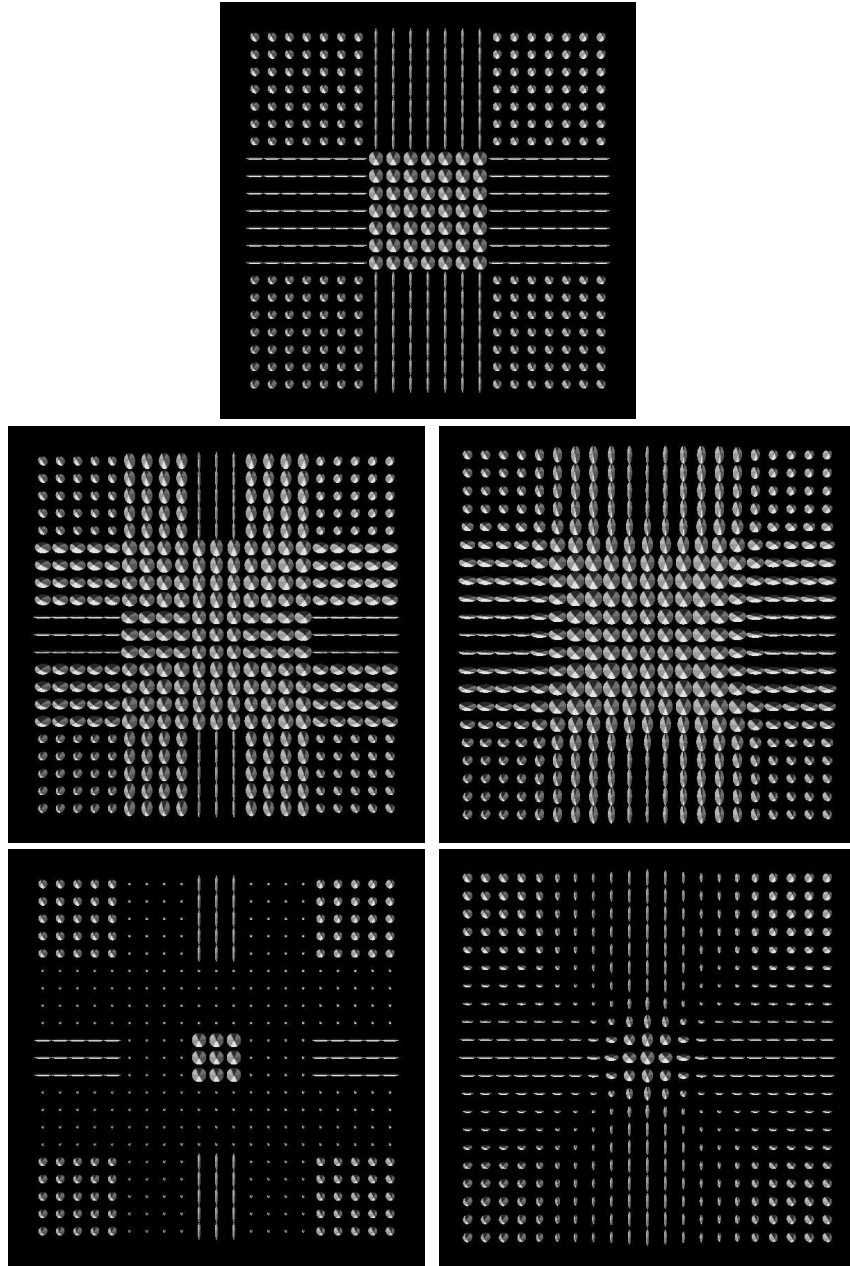


Figure 2: **(a) Top:** Central 2-D layer of an artificial 3-D positive definite matrix field. **(b) Middle left:** Dilation based on Loewner ordering. **(c) Middle right:** Dilation driven by PDE. **(d) Bottom left:** Erosion based on Loewner ordering. **(e) Bottom right:** Erosion driven by PDE. We chose the ball-shaped structuring element $BSE(2)$ and stopping time 2.

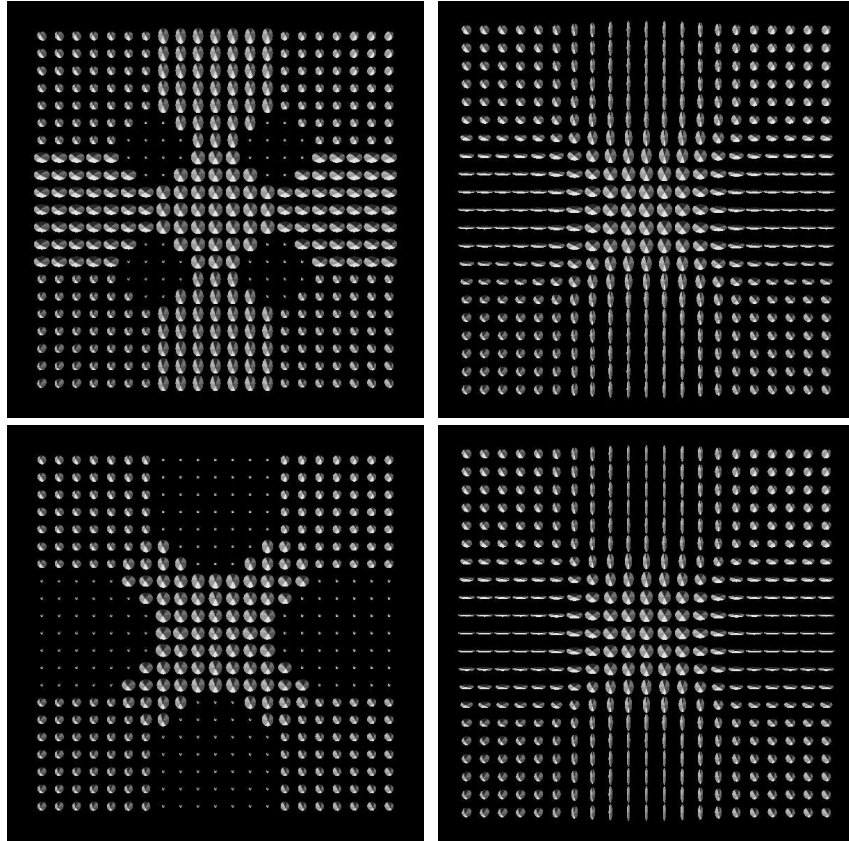


Figure 3: **(a) Top left:** Closing based on Loewner ordering. **(b) Top right:** Closing driven by PDE. **(c) Bottom left:** Opening based on Loewner ordering. **(d) Bottom right:** Opening driven by PDE. We chose the ball-shaped structuring element $BSE(2)$ and stopping time 2.

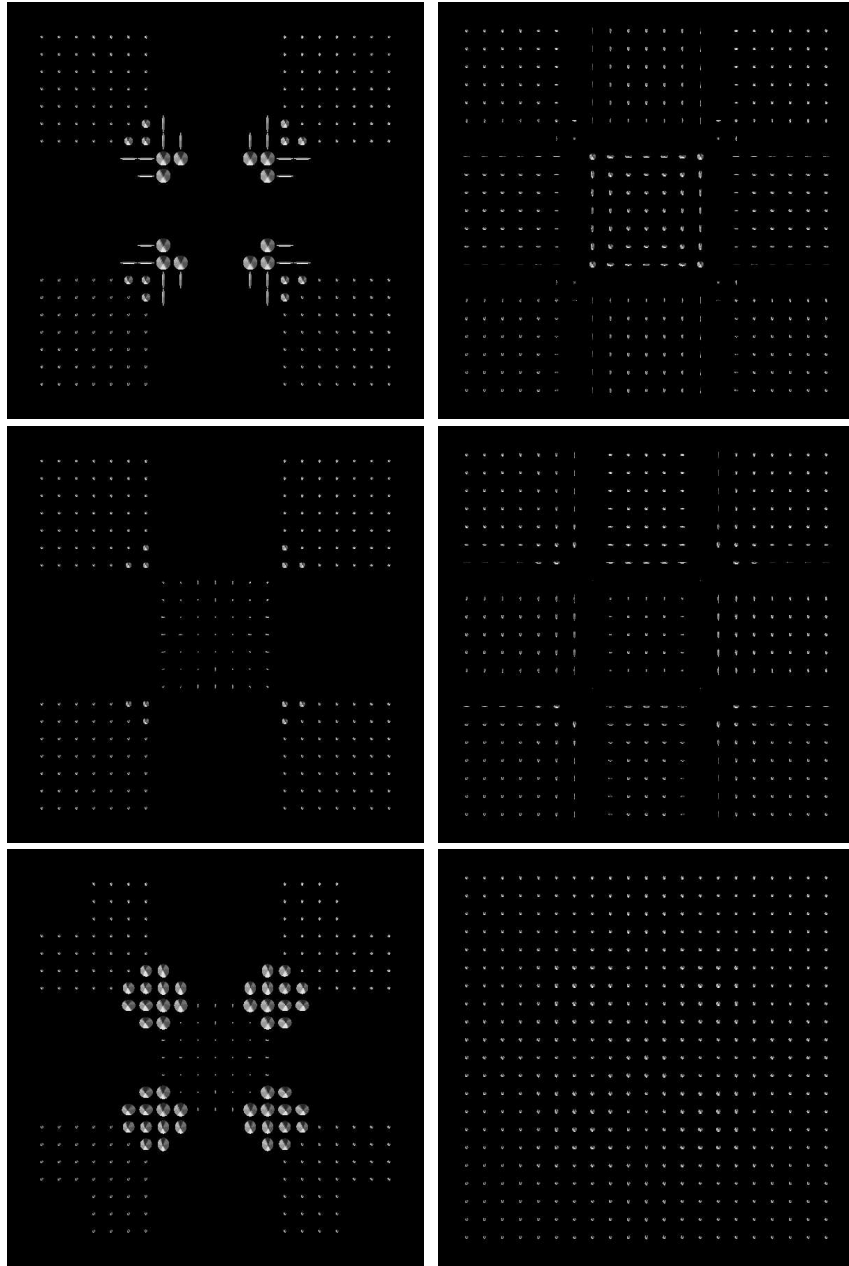


Figure 4: **(a) Top left:** WTH based on Loewner ordering. **(b) Top right:** WTH driven by PDE. **(c) Middle left:** BTH based on Loewner ordering. **(d) Middle right:** BTH driven by PDE. **(e) Bottom left:** SDTH based on Loewner ordering. **(f) Bottom right:** SDTH driven by PDE. We chose the ball-shaped structuring element $BSE(2)$ and stopping time 2.

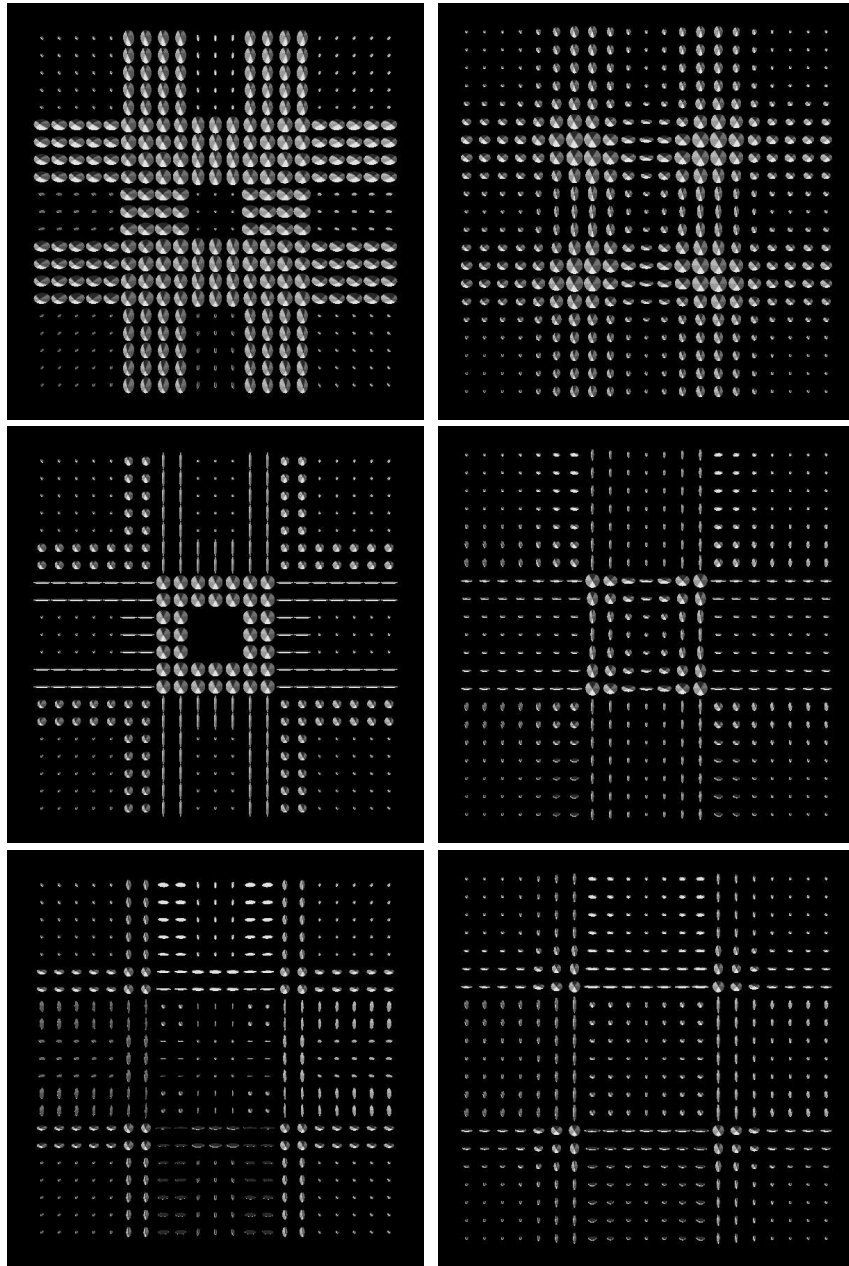


Figure 5: **(a) Top left:** Beucher gradient based on Loewner ordering. **(b) Top right:** Beucher gradient driven by PDE. **(c) Middle left:** Internal gradient based on Loewner ordering. **(d) Middle right:** Internal gradient driven by PDE. **(e) Bottom left:** External gradient based on Loewner ordering. **(f) Bottom right:** External gradient driven by PDE. We chose the ball-shaped structuring element BSE(2) and stopping time 2.

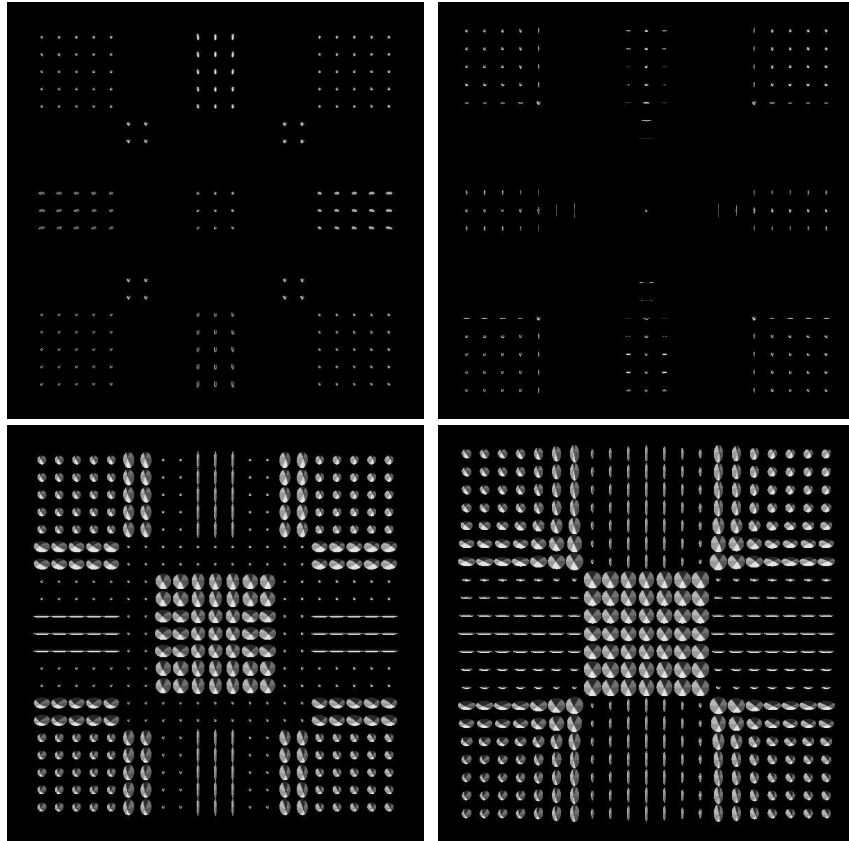


Figure 6: **(a) Top left:** Morphological Laplacian based on Loewner ordering. **(b) Top right:** Morphological Laplacian driven by PDE. **(c) Bottom left:** Shock filtering based on Loewner ordering. **(d) Bottom right:** Shock filtering driven by PDE. We chose the ball-shaped structuring element $BSE(2)$ and stopping time 2.

The Laplacian Δ_m which is computed as the difference of the external and internal gradient, produces positive definite matrices as well as indefinite and negative definite ones. This is the explanation for the void areas in the figures 6 (a) and 11 (b): Non-positive definite matrices cannot be displayed as ellipsoids and hence are omitted. The effect of the Laplacian Δ_B and its use for steering a shock filter can be seen in figures 6 and 11: While applying dilation in pixels where the trace of the Laplacian is negative, the shock filter acts as an erosion wherever the trace of the Laplacian is positive. The output are images where regions with larger and smaller eigenvalues are separated more clearly than in the original image. This is true for both approaches since there is a strong similarity between the corresponding results.

5 Conclusion

In this paper we have extended fundamental concepts of mathematical morphology to the case of 3-dimensional matrix-valued data by two completely different approaches.

Firstly, based on the Loewner ordering for symmetric matrices notions of maximum and minimum of a set of symmetric 3×3 -matrices have been proposed. These notions extend the corresponding scalar-valued concept. They exhibit invariance, positivity, and continuity properties essential for their use in the design of morphological operations for matrix-valued data. For this reason we have succeeded to generalise not only standard morphological operations but also morphological derivatives and shock filters to the matrix-valued setting. The technique holds the potential to cope with 4×4 -matrices or larger.

Secondly, we generalised the nonlinear PDEs that simulate erosion and dilation to the matrix-valued setting. The corresponding nonlinear system of PDEs provides a novel way to morphology for matrix fields.

Thirdly, in order to put these PDEs to use we introduced a matrix-valued version of the scalar Osher-Sethian-scheme as a numerical method to solve the proposed matrix-valued PDEs.

In the experimental part we have contrasted results achieved by the two approaches for standard morphological operations as well as morphological derivatives. Though completely different in their character the two methods lead to very similar results in the case of dilation, erosion, derivatives, and shock filtering. They feature the same characteristics as their scalar-valued counterparts.

The resemblance in the case of morphological operations that rely on the concatenation of dilation and erosion, namely closing, opening, and the top

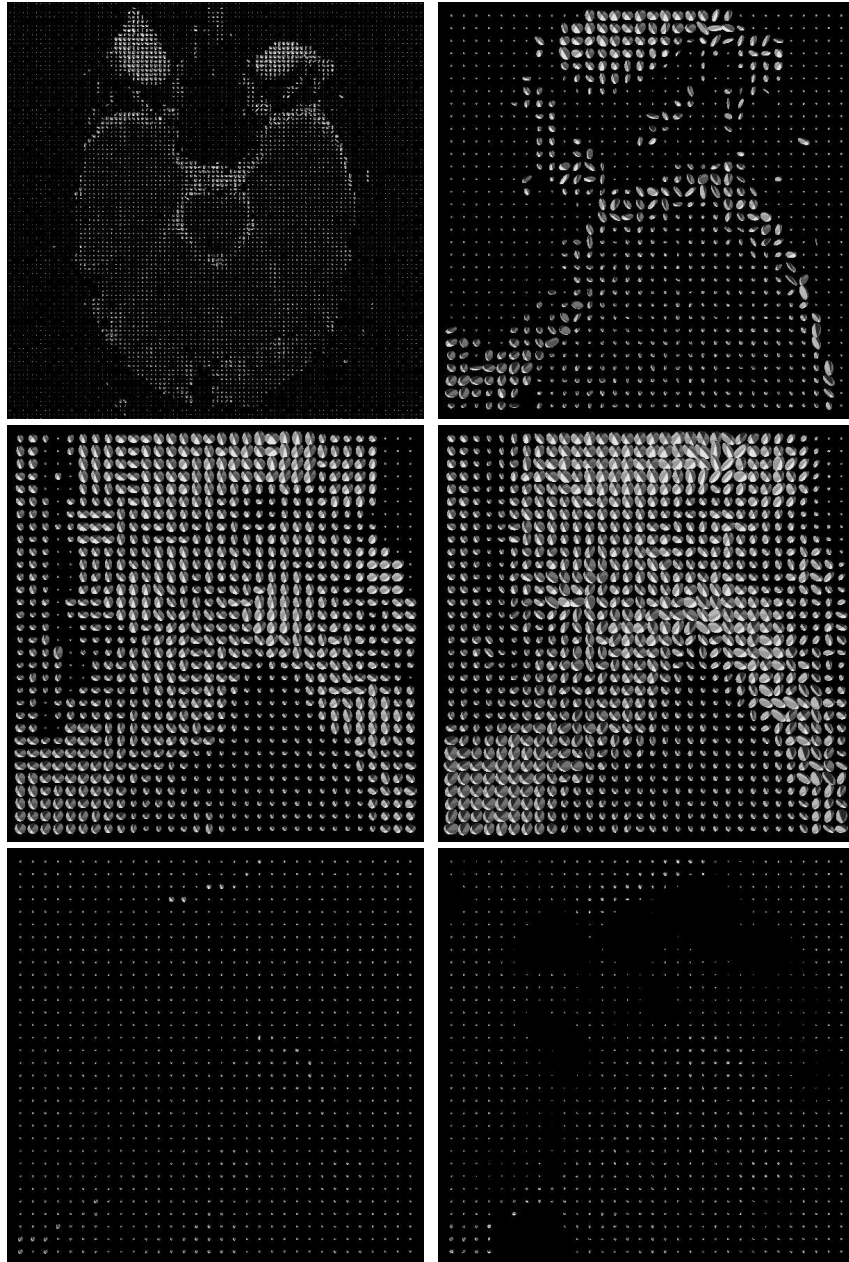


Figure 7: **(a) Top left:** A slice of a 3-D matrix field extracted from a DT-MRI data set of a human head. **(b) Top right:** Enlargement of a section in the upper right corner of (a). **(c) Middle left:** Dilation based on Loewner ordering. **(d) Middle right:** Dilation driven by PDE. **(e) Bottom left:** Erosion based on Loewner ordering. **(f) Bottom right:** Erosion driven by PDE. We chose the ball-shaped structuring element $BSE(2)$ and stopping time 2.

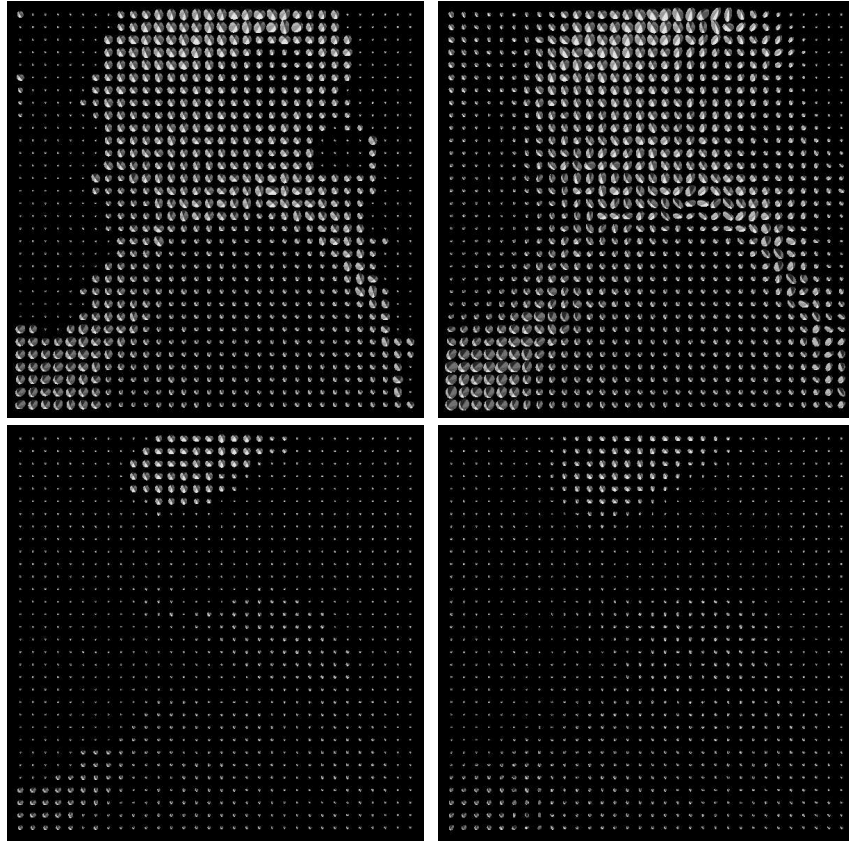


Figure 8: **(a) Top left:** Closing based on Loewner ordering. **(b) Top right:** Closing driven by PDE. **(c) Bottom left:** Opening based on Loewner ordering. **(d) Bottom right:** Opening driven by PDE. We chose the ball-shaped structuring element $BSE(2)$ and stopping time 2.

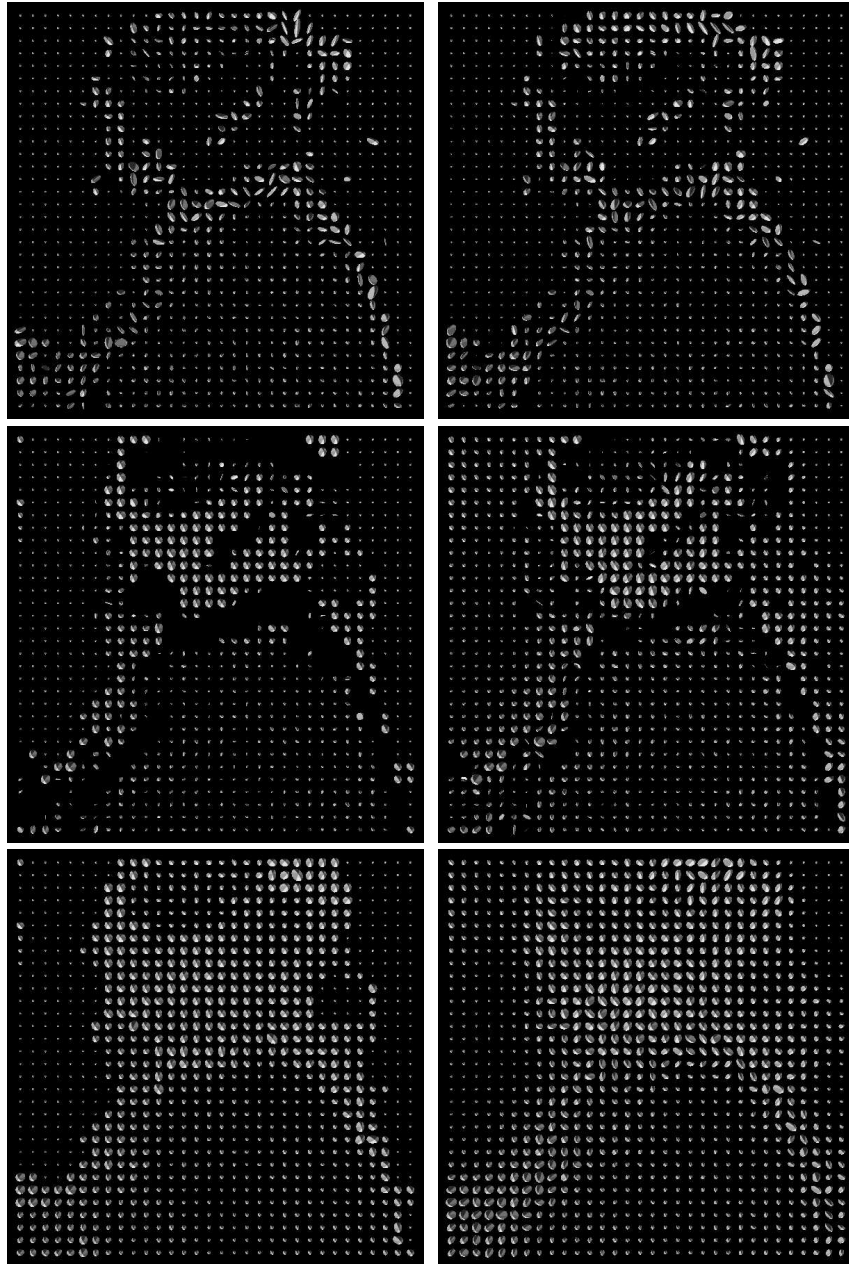


Figure 9: **(a) Top left:** WTH based on Loewner ordering. **(b) Top right:** WTH driven by PDE. **(c) Middle left:** BTH based on Loewner ordering. **(d) Middle right:** BTH driven by PDE. **(e) Bottom left:** SDTH based on Loewner ordering. **(f) Bottom right:** SDTH driven by PDE. We chose the ball-shaped structuring element $BSE(2)$ and stopping time 2.

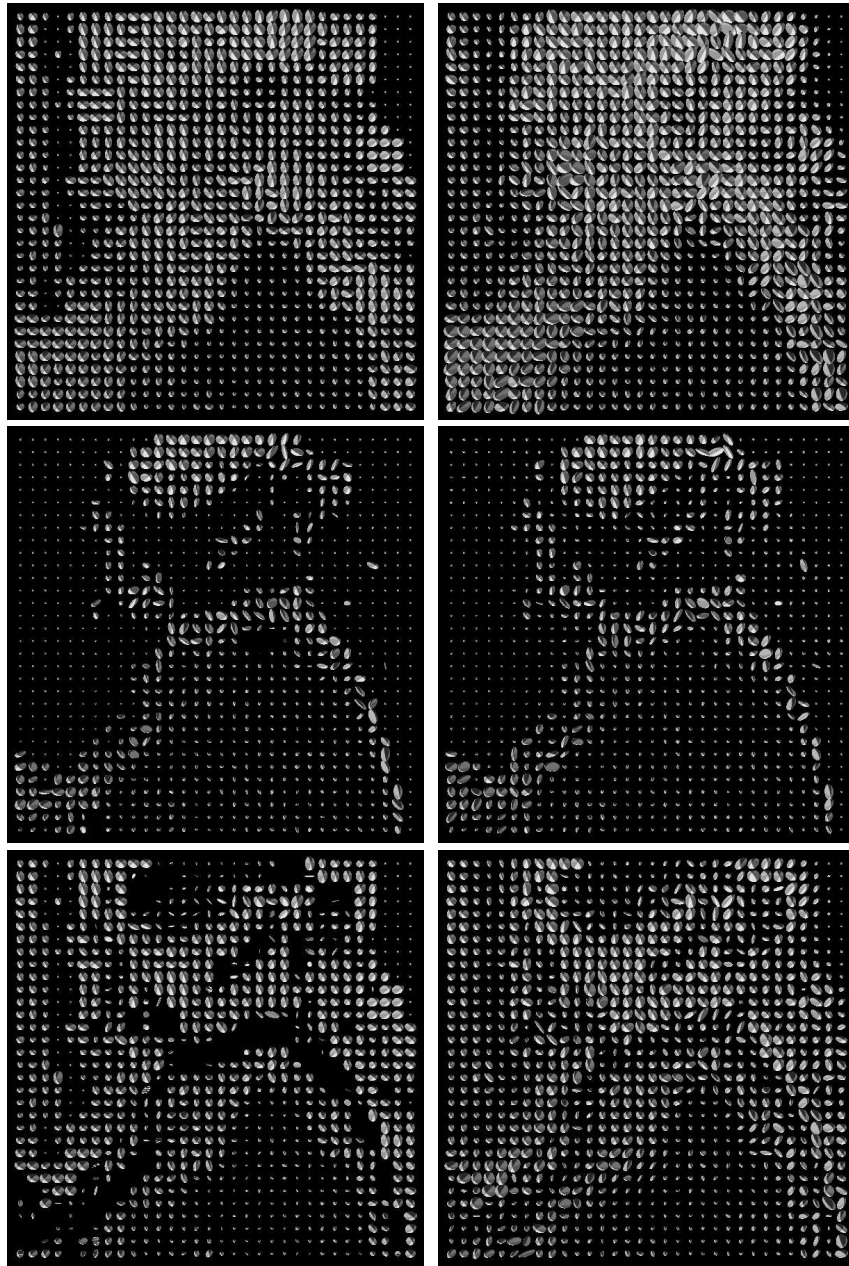


Figure 10: **(a) Top left:** Beucher gradient based on Loewner ordering. **(b) Top right:** Beucher gradient driven by PDE. **(c) Middle left:** Internal gradient based on Loewner ordering. **(d) Middle right:** Internal gradient driven by PDE. **(e) Bottom left:** External gradient based on Loewner ordering. **(f) Bottom right:** External gradient driven by PDE. We chose the ball-shaped structuring element BSE(2) and stopping time 2.



Figure 11: **(a) Top left:** Morphological Laplacian based on Loewner ordering. **(b) Top right:** Morphological Laplacian driven by PDE. **(c) Bottom left:** Shock filtering based on Loewner ordering. **(d) Bottom right:** Shock filtering driven by PDE. We chose the ball-shaped structuring element $BSE(2)$ and stopping time 2.

hat operators, is not as striking. We see the reason for that in the blurring effects caused by the Osher-Sethian scheme.

However, the development of discontinuity-preserving numerical schemes capable of capturing adequately the behaviour of morphological operations is work in progress.

Ongoing research comprises also the exploration of the potential of the PDE-driven approach involving speed functions. The development of more sophisticated morphological operations for matrix fields as well as methods to improve performance is work in progress.

References

- [1] D. C. Alexander. An Introduction to Computational Diffusion MRI: the Diffusion Tensor and Beyond. In J. Weickert and H. Hagen , editor, *Visualization and Processing of Tensor Fields*, pages 77–100. Springer, Berlin, 2006.
- [2] A. Barvinok. *A Course in Convexity*, volume 54 of *Graduate Studies in Mathematics*. American Mathematical Society, Providence, 2002.
- [3] P. J. Basser. Inferring microstructural features and the physical state of tissues from diffusion-weighted images. *Nuclear Magnetic Resonance in Biomedicine*, 8:333–334, 1995.
- [4] P. J. Basser, J. Mattiello, and D. LeBihan. MR diffusion tensor spectroscopy and imaging. *Biophysical Journal*, 66:259–267, 1994.
- [5] J. Bigün, G. H. Granlund, and J. Wiklund. Multidimensional orientation estimation with applications to texture analysis and optical flow. *IEEE Transactions on Pattern Analysis and Machine Intelligence*, 13(8):775–790, August 1991.
- [6] T. Brox, M. Rousson, R. Deriche, and J. Weickert. Unsupervised segmentation incorporating colour, texture, and motion. In N. Petkov and M. A. Westenberg, editors, *Computer Analysis of Images and Patterns*, volume 2756 of *Lecture Notes in Computer Science*, pages 353–360. Springer, Berlin, 2003.
- [7] T. Brox and J. Weickert. Nonlinear matrix diffusion for optic flow estimation. In L. Van Gool, editor, *Pattern Recognition*, volume 2449 of *Lecture Notes in Computer Science*, pages 446–453. Springer, Berlin, 2002.

- [8] B. Burgeth, N. Papenberg, A. Bruhn, M. Welk, C. Feddern, and J. Weickert. Mathematical morphology based on the loewner ordering for tensor data. In C. Ronse, L. Najman, and E. Decencière, editors, *Mathematical Morphology: 40 Years On*, volume 30 of *Computational Imaging and Vision*, pages 407–418. Springer, Dordrecht, 2005.
- [9] B. Burgeth, M. Welk, C. Feddern, and J. Weickert. Morphological operations on matrix-valued images. In T. Pajdla and J. Matas, editors, *Computer Vision – ECCV 2004*, volume 3024 of *Lecture Notes in Computer Science*, pages 155–167. Springer, Berlin, 2004.
- [10] B. Burgeth, M. Welk, C. Feddern, and J. Weickert. Mathematical morphology on tensor data using the loewner ordering. In H. Hagen J. Weickert, editor, *Visualization and Processing of Tensor Fields*. Springer, Berlin, 2005. to appear.
- [11] O. Coulon, D. C. Alexander, and S. A. Arridge. A regularization scheme for diffusion tensor magnetic resonance images. In M. F. Insana and R. M. Leahy, editors, *Information Processing in Medical Imaging – IPMI 2001*, volume 2082 of *Lecture Notes in Computer Science*, pages 92–105. Springer, Berlin, 2001.
- [12] C. Feddern, J. Weickert, B. Burgeth, and M. Welk. Curvature-driven pde methods for matrix-valued images. Technical Report 104, Department of Mathematics, Saarland University, Saarbrücken, Germany, May 2004.
- [13] W. Förstner and E. Gülch. A fast operator for detection and precise location of distinct points, corners and centres of circular features. In *Proc. ISPRS Intercommission Conference on Fast Processing of Photogrammetric Data*, pages 281–305, Interlaken, Switzerland, June 1987.
- [14] B. Gärtner. <http://www.inf.ethz.ch/personal/gaertner/>. WebPage last visited: December 10th, 2005.
- [15] J. Goutsias, H. J. A. M. Heijmans, and K. Sivakumar. Morphological operators for image sequences. *Computer Vision and Image Understanding*, 62:326–346, 1995.
- [16] J. Goutsias, L. Vincent, and D. S. Bloomberg, editors. *Mathematical Morphology and its Applications to Image and Signal Processing*, volume 18 of *Computational Imaging and Vision*. Kluwer, Dordrecht, 2000.

- [17] G. H. Granlund and H. Knutsson. *Signal Processing for Computer Vision*. Kluwer, Dordrecht, 1995.
- [18] K. Hahn, S. Pigarin, and B. Pütz. Edge preserving regularization and tracking for diffusion tensor imaging. In W. J. Niessen and M. A. Viergever, editors, *Medical Image Computing and Computer-Assisted Intervention – MICCAI 2001*, volume 2208 of *Lecture Notes in Computer Science*, pages 195–203. Springer, Berlin, 2001.
- [19] C. G. Harris and M. Stephens. A combined corner and edge detector. In *Proc. Fourth Alvey Vision Conference*, pages 147–152, Manchester, England, August 1988.
- [20] H. J. A. M. Heijmans. *Morphological Image Operators*. Academic Press, Boston, 1994.
- [21] H. J. A. M. Heijmans and J. B. T. M. Roerdink, editors. *Mathematical Morphology and its Applications to Image and Signal Processing*, volume 12 of *Computational Imaging and Vision*. Kluwer, Dordrecht, 1998.
- [22] J.-B. Hiriart-Urruty and C. Lemarechal. *Fundamentals of Convex Analysis*. Springer, Heidelberg, 2001.
- [23] R. A. Horn and C. R. Johnson. *Matrix Analysis*. Cambridge University Press, Cambridge, UK, 1990.
- [24] H. P. Kramer and J. B. Bruckner. Iterations of a non-linear transformation for enhancement of digital images. *Pattern Recognition*, 7:53–58, 1975.
- [25] G. Louverdis, M. I. Vardavoulia, I. Andreadis, and P. Tsalides. A new approach to morphological color image processing. *Pattern Recognition*, 35:1733–1741, 2002.
- [26] G. Matheron. *Éléments pour une théorie des milieux poreux*. Masson, Paris, 1967.
- [27] G. Matheron. *Random Sets and Integral Geometry*. Wiley, New York, 1975.
- [28] S. Osher and J. A. Sethian. Fronts propagating with curvature-dependent speed: Algorithms based on Hamilton–Jacobi formulations. *Journal of Computational Physics*, 79:12–49, 1988.

- [29] G. J. M. Parker, J. A. Schnabel, M. R. Symms, D. J. Werring, and G. J. Barker. Nonlinear smoothing for reduction of systematic and random errors in diffusion tensor imaging. *Journal of Magnetic Resonance Imaging*, 11:702–710, 2000.
- [30] C. Pierpaoli, P. Jezzard, P. J. Basser, A. Barnett, and G. Di Chiro. Diffusion tensor MR imaging of the human brain. *Radiology*, 201(3):637–648, December 1996.
- [31] A. R. Rao and B. G. Schunck. Computing oriented texture fields. *CVGIP: Graphical Models and Image Processing*, 53:157–185, 1991.
- [32] M. Rousson, T. Brox, and R. Deriche. Active unsupervised texture segmentation on a diffusion based feature space. In *Proc. 2003 IEEE Computer Society Conference on Computer Vision and Pattern Recognition*, volume 2, pages 699–704, Madison, WI, June 2003. IEEE Computer Society Press.
- [33] G. Sapiro. *Geometric Partial Differential Equations and Image Analysis*. Cambridge University Press, Cambridge, UK, 2001.
- [34] G. Sapiro, R. Kimmel, D. Shaked, B. B. Kimia, and A. M. Bruckstein. Implementing continuous-scale morphology via curve evolution. *Pattern Recognition*, 26:1363–1372, 1993.
- [35] J. Serra. *Echantillonnage et estimation des phénomènes de transition minier*. PhD thesis, University of Nancy, France, 1967.
- [36] J. Serra. *Image Analysis and Mathematical Morphology*, volume 1. Academic Press, London, 1982.
- [37] J. Serra. *Image Analysis and Mathematical Morphology*, volume 2. Academic Press, London, 1988.
- [38] P. Soille. *Morphological Image Analysis*. Springer, Berlin, 1999.
- [39] H. Talbot and R. Beare, editors. *Proc. Sixth International Symposium on Mathematical Morphology and its Applications*. Sydney, Australia, April 2002. <http://www.cmis.csiro.au/ismm2002/proceedings/>.
- [40] D. Tschumperlé and R. Deriche. Diffusion tensor regularization with constraints preservation. In *Proc. 2001 IEEE Computer Society Conference on Computer Vision and Pattern Recognition*, volume 1, pages 948–953, Kauai, HI, December 2001. IEEE Computer Society Press.

- [41] L. J. van Vliet, I. T. Young, and A. L. D. Beckers. A nonlinear Laplace operator as edge detector in noisy images. *Computer Vision, Graphics and Image Processing*, 45(2):167–195, 1989.
- [42] J. Weickert and T. Brox. Diffusion and regularization of vector- and matrix-valued images. In M. Z. Nashed and O. Scherzer, editors, *Inverse Problems, Image Analysis, and Medical Imaging*, volume 313 of *Contemporary Mathematics*, pages 251–268. AMS, Providence, 2002.
- [43] M. Welk, C. Feddern, B. Burgeth, and J. Weickert. Median filtering of tensor-valued images. In B. Michaelis and G. Krell, editors, *Pattern Recognition*, volume 2781 of *Lecture Notes in Computer Science*, pages 17–24, Berlin, 2003. Springer.
- [44] C.-F. Westin, S. E. Maier, B. Khidhir, P. Everett, F. A. Jolesz, and R. Kikinis. Image processing for diffusion tensor magnetic resonance imaging. In C. Taylor and A. Colchester, editors, *Medical Image Computing and Computer-Assisted Intervention – MICCAI 1999*, volume 1679 of *Lecture Notes in Computer Science*, pages 441–452. Springer, Berlin, 1999.